POAC'23
Glasgow, United Kingdom

Proceedings of the 27th International Conference on
Port and Ocean Engineering under Arctic Conditions
12-16 June 2023, Glasgow, United Kingdom

Modelling the Mechanical response of Single Crystal S2 Ice using Non-Ordinary State-Based Peridynamics

Yakubu K. Galadima[1,2], Erkan Oterkus[1], Selda Oterkus[1]

[1]PeriDynamics Research Centre, Department of Naval Architecture, Ocean and Marine Engineering, University of Strathclyde, Glasgow, United Kingdom

[2]Department of Civil Engineering, Ahmadu Bello University, Zaria, Nigeria

ABSTRACT

This study presents a new approach to model single crystal S2 ice using Non-Ordinary State-Based Peridynamic (NOSBPD) theory. The proposed NOSBPD model presents the advantage of admitting constitutive models from the classical continuum theory while retaining the advantages of the peridynamic theory. To validate the proposed model, numerical simulations were performed, and the results obtained show good agreement with those obtained from numerical simulation done in the framework of Finite Element Method (FEM).

KEYWORDS: Non-ordinary state-based peridynamics; Nonlocal; S2 Ice.

1.0 INTRODUCTION

The significance of ice shelf fracture processes, the impact of ice-structure interaction on ships and offshore structures, and their implications for ice sheet dynamics and climate are strong motivations for the development of mathematical models capable of capturing the complex behaviour of ice. Such models are crucial for predicting and analysing the behaviour of ice under various loading conditions, allowing for the design and engineering of structures that can withstand the challenges posed by ice.

Models based on the classical continuum theory have proven to be inadequate in capturing some behaviours exhibited by ice, such as ice fracture, and granular flow. Classical continuum mechanics (CCM) models rely on spatial partial derivatives to describe the behaviour of materials. However, these models are ill-suited for discontinuous systems, such as fractured ice, as spatial partial derivatives are not well-defined at discontinuities. As a result, CCM models fail to accurately capture the complex fracture processes and discontinuous behaviour that often arise in ice dynamics.

Moreover, granular flow in ice has been observed to exhibit size-dependent behaviour. This size-effect arises due to the finite size of ice grains compared to the larger scale of the flow environment. CCM models are unable to capture this size-effect and the resulting changes in the behaviour of granular ice flow (West et al., 2022).

These limitations highlight the need for alternative approaches that can overcome the challenges posed by nonlocal effects and behaviours in ice. One promising alternative is the utilization of nonlocal continuum models, such as peridynamics (Silling, 2000), which can capture the nonlocal interactions and discontinuous behaviour exhibited by ice. By considering the long-range interactions between particles, nonlocal models offer a more suitable framework for accurately describing and predicting the fracture processes and granular flow in ice.

Peridynamics has emerged as a powerful tool for solving a wide range of engineering problems. It has found extensive applications as the theoretical foundation for numerical investigations

of fracture evolution and propagation (Nguyen & Oterkus, 2020), as well as impact dynamics (Oterkus, Guven, et al., 2012). Peridynamics has also been utilized to study composite materials (Oterkus, Madenci, et al., 2012), functionally graded materials and viscoelastic materials (Galadima et al., 2023a). To improve computational efficiency, various model reduction techniques have been proposed for peridynamics, including the coarsening method (Galadima et al., 2019; Galadima et al., 2021; Silling, 2011) and model reduction based on static condensation (Galadima et al., 2020b; Galadima, Oterkus, et al., 2022). Furthermore, to extend the applicability of peridynamics to characterize the effective behaviour of heterogeneous media, several homogenization theories have been developed (Buryachenko, 2019; Galadima et al., 2020a; Galadima et al., 2023b; Galadima, Xia, et al., 2022; Xia et al., 2019; Xia et al., 2021). These advancements in peridynamics contribute to its potential for addressing complex engineering challenges across different disciplines.

Several research efforts have been expended to develop models for ice within the peridynamic framework. A bond-based peridynamic model to model polycrystalline ice was proposed in (Lu et al., 2020). The proposed model was used to carry out a dynamic analysis of a polycrystalline ice material with two pre-existing cracks under tension loading. Similarly, the bond-based model was used in (Vazic et al., 2020) to calculate in-plane splitting loads for several differently sized ice plates. An ordinary state-based peridynamic formulation was proposed in (Li et al., 2023) to model the behaviour of polycrystalline S2 columnar ice. In (Xue et al., 2019), a framework to characterise ice-ship interaction was proposed. The proposed framework utilised the bond-based model of ice to determine the ice loads for a ship navigating in level ice. In a similar work, the NOSBPD framework was utilised in (Liu et al., 2017) to simulate interaction of level ice and vertical structure. In (Song et al., 2019), a NOSBPD was to simulate water ice crater formation due to impact loads utilizing modified Drucker-Prager constitutive model.

In this paper, we propose an approach based on the NOSBPD correspondence framework, to model the response of a single crystal S2 ice. By incorporating nonlocal phenomena and capturing the complex interactions within ice structures, this model offers a promising avenue for gaining deeper insights into ice mechanics. Through the development and application of this model, we aim to contribute to the understanding of ice shelf fracture, ice-structure interaction, and their implications for climate dynamics, providing valuable tools for the design and assessment of ice-related structures and systems.

2.0 THEORETICAL FRAMEWORK OF THE NOSBPD MODEL

The peridynamics framework is a nonlocal continuum mechanics formulation that introduces integral operators to replace the spatial differential operators found in the classical theory. By utilizing integral operators in the governing equations, peridynamics removes the requirement of continuity in the system's response that is necessary in classical theories. The peridynamic equation of motion of a point $\mathbf{x}$ in a body as it interacts with other points $\mathbf{x}'$ within the body is given by the following balance of linear momentum expression:

$$\rho(\mathbf{x})\ddot{\boldsymbol{u}}(\mathbf{x},t) = \int_{\mathcal{H}_{\mathbf{x}}} \mathbf{f}(\mathbf{x},\mathbf{x}',t)\, dV_{\mathbf{x}'} + \mathbf{b}(\mathbf{x},t) \tag{1}$$

Here, $\rho(\mathbf{x})$ represents the material density at $\mathbf{x}$, $\ddot{\boldsymbol{u}}$ denotes the second order derivative of the displacement $(\boldsymbol{u})$ of $\mathbf{x}$ with respect to time (t), $\mathbf{b}(\mathbf{x},t)$ is the body force at point $\mathbf{x}$, $\mathbf{f}(\mathbf{x},\mathbf{x}',t)$ is a vector-valued pairwise nonlocal force density that the material point $\mathbf{x}'$ exerts on material point at position $\mathbf{x}$. This nonlocal force density is transmitted through the notion of a *bond* which represent the interaction between two material points $\mathbf{x}$ and $\mathbf{x}'$ separated by a finite distance $\mathbf{x}' - \mathbf{x} = \boldsymbol{\xi}$ in the undeformed configuration called the *bond length*. The bond length

is sometimes referred to simply as bond for brevity with its exact meaning discerned from the context.

In (1), $\mathcal{H}$ is the set of all points $\mathbf{x}'$ in the body that interacts with $\mathbf{x}$. The size of this set varies depending on the specific physics being studied, ranging from a few neighbouring points to encompassing all points within the body. In most literature on peridynamics, this set is called the family of $\mathbf{x}$ and is defined to include all points laying within a given radius from the primary point. This radius often denoted as δ is called the *horizon*. The horizon is seen as an internal length parameter that determines the extent of nonlocal interaction allowed in the system.

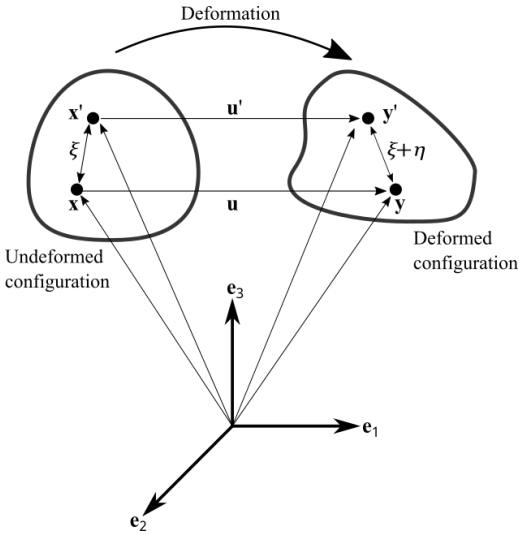

Figure 1: Deformation of material point

During deformation, if $\mathbf{x}$ and $\mathbf{x}'$ now occupy locations $\mathbf{y}$ and $\mathbf{y}'$ respectively, in the deformed configuration, and let $\mathbf{u}$ and $\mathbf{u}'$ represent the respective displacement of $\mathbf{x}$ and $\mathbf{x}'$ during this deformation as shown in Figure 1. Then the relative displacement and relative position vector of $\mathbf{x}$ and $\mathbf{x}$ are respectively given as:

$$\boldsymbol{\eta} = \mathbf{u}' - \mathbf{u}, \qquad \mathbf{y}' - \mathbf{y} = \boldsymbol{\xi} + \boldsymbol{\eta} \tag{2}$$

The integral representation of the balance law as given by (1) allows for the modelling of both continuous and discontinuous responses in engineering systems. The definition of the force density function $\boldsymbol{f}(\boldsymbol{x}, \boldsymbol{x}')$ in (1) give rise to three different types of models. The first peridynamic model is the bond-based model (Silling, 2000) in which the force density function $\boldsymbol{f}(\boldsymbol{x}, \boldsymbol{x}')$ is defined as a function of only the bond $\boldsymbol{x}' - \boldsymbol{x}$ and is independent of the deformation of any other bond within the family of the primary point $\mathbf{x}$. This definition of the force density leads to a peridynamic model that is simple and computationally efficient to implement on one hand, and on the other restrict the types of materials that can be modelled to those with Poisson's ratio of 1/3 and 1/4 for 2- and 3-dimensional problems respectively.

To mitigate against this restriction, a state-based peridynamic framework was proposed (Silling et al., 2007) as a framework with more generalised capabilities for material modelling. In the state-based framework, the force density $\boldsymbol{f}(\boldsymbol{x}, \boldsymbol{x}')$ is a function of not just the bond $\boldsymbol{x}' - \boldsymbol{x}$, but of all bonds within $\mathcal{H}_{\mathbf{x}}$. This extended capability is achieved by the introduction of mathematical objects called *states* which allows the recasting of the peridynamic equation of motion (1) as

$$\rho(\mathbf{x})\ddot{\boldsymbol{u}}(\mathbf{x}, t) = \int_{\mathcal{H}_{\mathbf{x}}} \{\underline{\mathbf{T}}[\mathbf{x}, t]\langle \mathbf{x}' - \mathbf{x}\rangle - \underline{\mathbf{T}}[\mathbf{x}', t]\langle \mathbf{x} - \mathbf{x}'\rangle \, dV_{\mathbf{x}'} + \mathbf{b}(\mathbf{x}, t) \tag{3}$$

where $\underline{\mathbf{T}}$ is defined as the vector force state at $\mathbf{x}$ in time t. When $\underline{\mathbf{T}}$ acts on the bond $\mathbf{x}' - \mathbf{x}$, the result is the vector-valued force density function $\mathbf{t}(\mathbf{x}, \mathbf{x}', t)$ acting on $\mathbf{x}'$ due to its interaction with the point $\mathbf{x}$. Two types of material models emerge from the state-based framework (3) depending on the definition of the force state $\underline{\mathbf{T}}$. If the force state $\underline{\mathbf{T}}$ is defined such that the force density $\mathbf{t}(\mathbf{x}, \mathbf{x}', t)$ is colinear with the bond $\boldsymbol{\xi} = \mathbf{x}' - \mathbf{x}$, then $\underline{\mathbf{T}}$ is said to be an ordinary state, giving rise to the so-called ordinary state-based peridynamic model, otherwise $\underline{\mathbf{T}}$ is a non-ordinary state and give rise to the NOSBPD model.

the NOSBPD model allow for a more generalised material model. Furthermore, a class of the NOSBPD models called the peridynamic correspondence model provide a framework that allow material models from the classical continuum theory to be use within the peridynamic framework thus making it possible to leverage the advantages of both frameworks. In the correspondence model, the force state $\underline{\mathbf{T}}$ is defined such that:

$$\underline{\boldsymbol{T}}[\boldsymbol{x}, t]\langle\boldsymbol{\xi}\rangle = \omega(|\boldsymbol{\xi}|)\mathbf{P}\mathbf{K}^{-1}\boldsymbol{\xi} \tag{4}$$

In (4), ω is a scalar-valued influence function which measures the impact that the deformed bond $\boldsymbol{\xi}$ has on the force field at $\mathbf{x}$, $\mathbf{P} = \widehat{\mathbf{P}}(\mathbf{F})$ is the first Piola-Kirchhoff stress tensor obtained through the material model $\widehat{\mathbf{P}}$ from the classical theory as a function of the deformation gradient $\boldsymbol{F}$. The First Piola-Kirchhoff stress is related to the Cauchy stress tensor $\boldsymbol{\sigma}$ through the expression:

$$\mathbf{P} = J\boldsymbol{\sigma}\mathbf{F}^{-T}, \qquad J = \det(\mathbf{F}) \tag{5}$$

which in the context of small perturbation hypothesis we have $\mathbf{F} \cong \mathbf{I}$, $J \cong 1$ and thus $\mathbf{P} = \boldsymbol{\sigma}$ in (5) and consequently (4) can be written as:

$$\underline{\mathbf{T}}[\mathbf{x}, t]\langle\boldsymbol{\xi}\rangle = \omega(|\boldsymbol{\xi}|)\boldsymbol{\sigma}\mathbf{K}^{-1}\boldsymbol{\xi} \tag{6}$$

In (4) and (6), $\mathbf{K}$ is a second order shape tensor defined as

$$\mathbf{K} = \int_{\mathcal{H}_{\boldsymbol{x}}} \underline{\omega}\langle\boldsymbol{\xi}\rangle\, \boldsymbol{\xi}\otimes\boldsymbol{\xi} d\boldsymbol{V}_{\boldsymbol{\xi}} \tag{7}$$

The nonlocal approximation of the deformation gradient $\mathbf{F}$ is given by the expression:

$$\mathbf{F}(\mathbf{x}) = \left[\int_{\mathcal{H}_{\mathbf{x}}} \underline{\omega}\langle\boldsymbol{\xi}\rangle\big(\mathbf{y}(\mathbf{x}', t) - \mathbf{y}(\mathbf{x}, t)\big)\otimes\boldsymbol{\xi} d\mathbf{x}'\right]\mathbf{K}^{-1} \tag{8}$$

3.0 IMPLEMENTATION OF THE NOSBPD MODEL FOR ICE MECHANICS

The solution of the governing equation of motion (3) is often obtained numerically. To set up the problem for numerical implementation, the problem domain is discretised into a set of nodes and then numerical methods such as the FEM (Chen & Gunzburger, 2011; Wang & Tian, 2012), meshfree methods (Parks et al., 2008; Silling & Askari, 2005) and collocation methods (Evangelatos & Spanos, 2011; Wang & Tian, 2014) are used to approximate the solution. The meshfree method proposed in (Silling & Askari, 2005) is utilised in this contribution due to its simple implementation algorithm and relatively low computational cost. By employing this approximation method, the discrete form of (3) is obtained as

$$\rho_i\ddot{\mathbf{u}}_{\boldsymbol{i}} = \sum_{j=1}^{N}\left[\underline{\mathbf{T}}[\mathbf{x}_i, t]\langle\mathbf{x}_j - \mathbf{x}_i\rangle - \underline{\mathbf{T}}\big[\mathbf{x}_j, t\big]\langle\mathbf{x}_i - \mathbf{x}_j\rangle\right]V_j + \boldsymbol{b}_{\boldsymbol{i}} \tag{9}$$

where N denotes the number of nodes in the family of $\mathbf{x}$.

4.0 ELASTICITY FOR SINGLE CRYSTAL ICE

In developing the ice model in this communication, the single ice crystal is assumed to obey the Hooke's law which assumes a linear relationship between stress and strain in the form:

$$\boldsymbol{\sigma} = \mathbf{C}\boldsymbol{\varepsilon} \tag{10}$$

where $\mathbf{C}$ is the fourth order elasticity tensor whose components C_{ij} $(i, j = 1 \text{ to } 6)$ are called the elastic or stiffness constants. Due to symmetry considerations, the independent components C_{ij} of the stiffness tensors reduces from 81 to 21for a generally anisotropic elastic material. Being a crystal with hexagonal symmetry, the elastic stiffness tensor of the S2 columnar ice is transversely isotropic thus further reducing the number of independent components C_{ij} to five. Utilizing the Voigt notation, the 3-D elastic stiffness tensor $\mathbf{C}^{3\mathrm{D}}$ for the S2 columnar ice can be written as (Elvin, 1996):

$$\begin{bmatrix} \mathrm{C}_{11}^{3D} & \mathrm{C}_{12}^{3D} & \mathrm{C}_{12}^{3D} & 0 & 0 & 0 \\ & \mathrm{C}_{22}^{3D} & \mathrm{C}_{13}^{3D} & 0 & 0 & 0 \\ & & \mathrm{C}_{22}^{3D} & 0 & 0 & 0 \\ & & & 1/2(\mathrm{C}_{22}^{3D} - \mathrm{C}_{13}^{3D}) & 0 & 0 \\ & \text{Sym} & & & \mathrm{C}_{55}^{3D} & 0 \\ & & & & & \mathrm{C}_{55}^{3D} \end{bmatrix} \tag{11}$$

If for practical convenience, it is assumed that plane stress condition applies, then the stiffness tensor in two-dimension is given as:

$$\begin{bmatrix} \mathrm{C}_{11}^{2D} & \mathrm{C}_{12}^{2D} & 0 \\ \mathrm{C}_{12}^{2D} & \mathrm{C}_{22}^{2D} & 0 \\ 0 & 0 & \mathrm{C}_{33}^{2D} \end{bmatrix} \tag{12}$$

Such that the components C_{ij}^{2D} of the stiffness tensor are obtained according to the following relation (Elvin, 1996):

$$\mathrm{C}_{11}^{2D} = \mathrm{C}_{11}^{3D} - \frac{\mathrm{C}_{13}^{3D}\mathrm{C}_{31}^{3D}}{\mathrm{C}_{33}^{3D}}, \quad \mathrm{C}_{12}^{2D} = \mathrm{C}_{12}^{3D} - \frac{\mathrm{C}_{13}^{3D}\mathrm{C}_{32}^{3D}}{\mathrm{C}_{33}^{3D}}, \quad \mathrm{C}_{21}^{2D} = \mathrm{C}_{21}^{3D} - \frac{\mathrm{C}_{23}^{3D}\mathrm{C}_{31}^{3D}}{\mathrm{C}_{33}^{3D}}$$
$$\mathrm{C}_{22}^{2D} = \mathrm{C}_{22}^{3D} - \frac{\mathrm{C}_{23}^{3D}\mathrm{C}_{32}^{3D}}{\mathrm{C}_{33}^{3D}}, \quad \mathrm{C}_{33}^{2D} = \mathrm{C}_{33}^{3D} \tag{13}$$

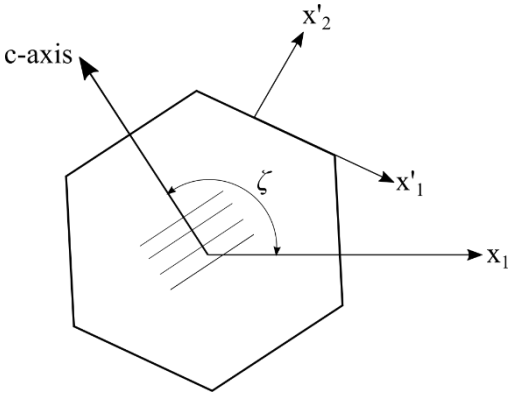

Figure 2: Schematic representation of ice showing crystal geometry.

It is worth noting that the material tensors (11) and (12) are specified with respect to the local axes of the crystal as shown in Figure 2. It is however sometimes necessary to transform the

components of the material tensor into a global axes system. In a two dimensional problem, the components of the fourth order stiffness tensor transform according to the following rule (Elvin, 1996):

$$\mathbf{C}_G = \boldsymbol{R}^T \mathbf{C}_\mathrm{L} \boldsymbol{R} \tag{14}$$

where the subscripts G and L denote global and local values respectively, and $\boldsymbol{R}$ is the transformation tensor given by:

$$\boldsymbol{R} = \begin{bmatrix} \cos^2(\zeta) & \sin^2(\zeta) & \frac{1}{2}\sin(2\zeta) \\ \sin^2(\zeta) & \cos^2(\zeta) & -\frac{1}{2}\sin(2\zeta) \\ -\sin(2\zeta) & \sin(2\zeta) & \cos(2\zeta) \end{bmatrix} \tag{15}$$

with ζ representing the angle between the c-axis of a crystal and the global $\mathbf{x}_1$.

5.0 NUMERICAL VALIDATION OF MODEL

In this section, we present the numerical simulation results for the monocrystalline ice. The ice crystal under investigation is assumed to have a square shape with dimensions of 1.2mm. A constant displacement $\mathbf{u}^o = \mathbf{x}_2^o \boldsymbol{\varepsilon}^o$ is applied to the top edge, where $\mathbf{x}_2^o$ represent the coordinates of the top boundary nodes in the $\mathbf{x}_2$ direction and $\boldsymbol{\varepsilon}^o = 1 \times 10^{-3}$ is a constant strain. The bottom edge is fixed as shown in Figure 3. The dynamic elastic stiffness tensor of the ice crystal, obtained from (Elvin, 1996), is given by (16) with the c-axis of the crystal inclined at an angle of 45^o with the global $\mathbf{x}_1$ axis. Plane stress condition is assumed to apply.

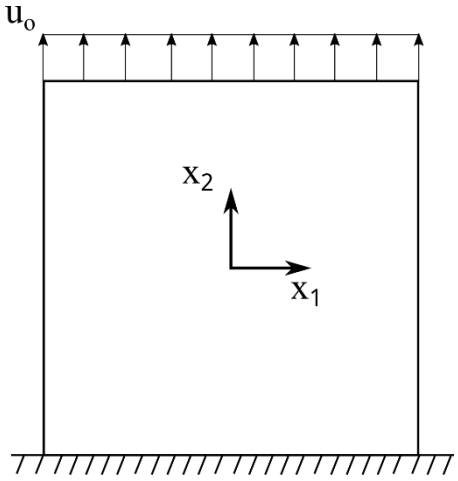

Figure 3: Schematic diagram of single ice crystal for numerical simulation

$$\begin{bmatrix} 15.010 & 5.765 & 5.765 & 0 & 0 & 0 \\ & 13.929 & 7.082 & 0 & 0 & 0 \\ & & 13.929 & 0 & 0 & 0 \\ & & & 3.4235 & 0 & 0 \\ & \mathrm{Sym} & & & 3.014 & 0 \\ & & & & & 3.014 \end{bmatrix} \mathrm{GPa} \tag{16}$$

The numerical implementation of the problem proceeds by discretizing the ice crystal into 200 nodes along each edge. A peridynamic horizon size of $3\Delta x$ is adopted where Δx is the size of the grid spacing. Since plane stress condition applies, we utilise equation (13) to reduce the stiffness tensor to obtain:

$$\begin{bmatrix} 12.624 & 2.832 & 0 \\ 2.832 & 10.328 & 0 \\ 0 & 0 & 3.014 \end{bmatrix} \text{GPa} \tag{17}$$

then use equation (3) to transform the stiffness tensor to the appropriate global frame.

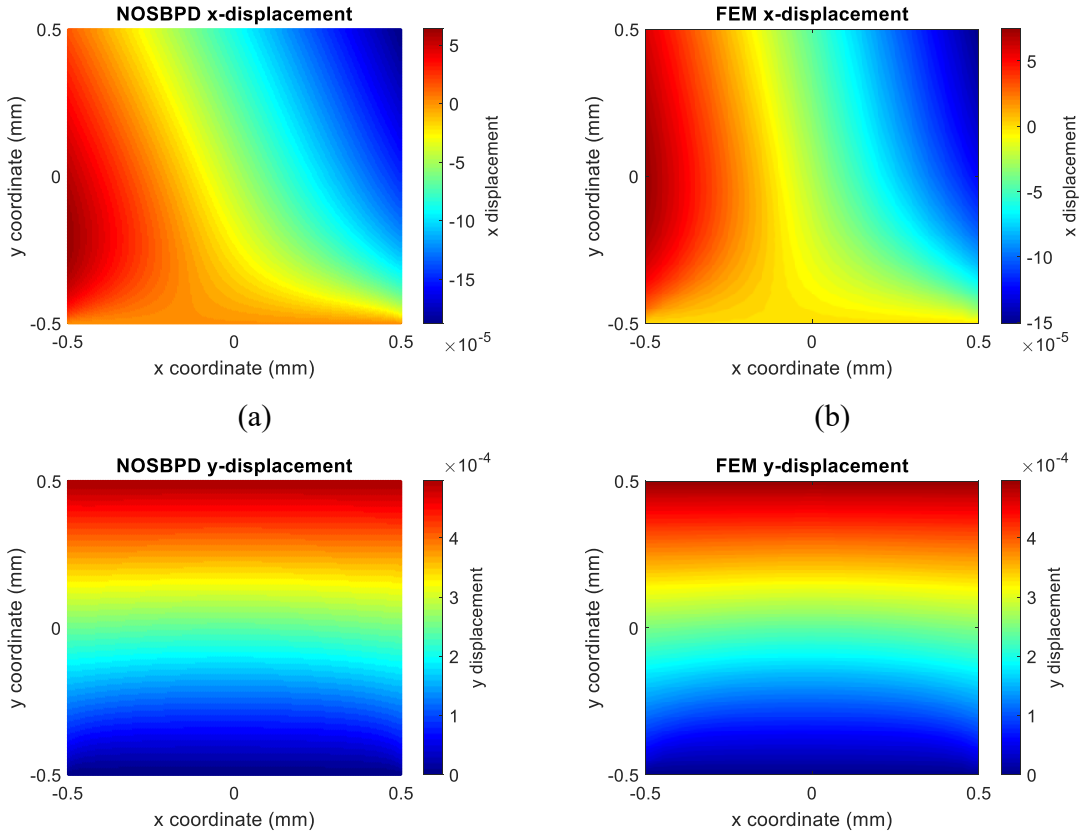

Figure 4: Results showing displacement fields: (a) displacement fields in x-direction from NOSBPD simulation, (b) displacement fields in x-direction from FEM simulation, (c) displacement fields in y-direction from NOSBPD simulation, (d) displacement fields in y-direction from FEM simulation.

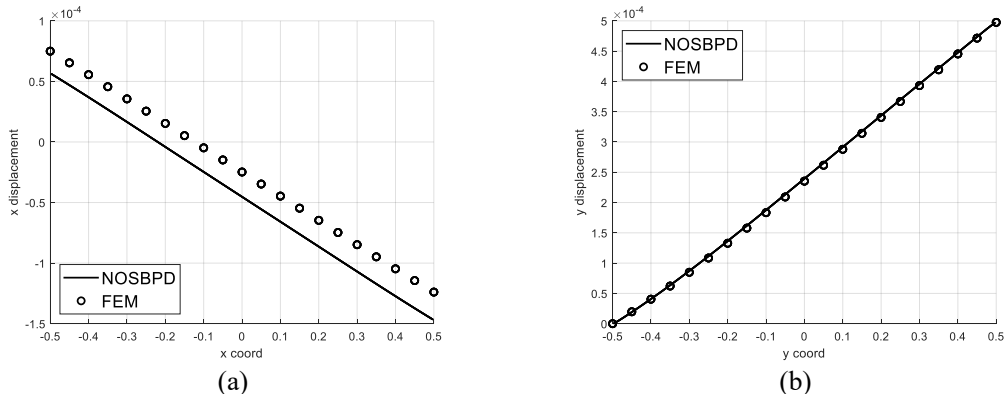

Figure 5: Profile of displacement along (a) a grid line of points in the x-direction, and (b) a grid line of points in the y-direction.

The results of the simulation using the proposed model of ice are presented in

Figure 4 and Figure 5.

Figure 4-a shows the displacement field in the x-direction within the ice crystal based on the proposed NOSBPD model, and for comparison purposes,

Figure 4-b shows the x-direction field of displacement as obtained by finite element (FE) simulation.

Figure 4-c on the other hand shows the corresponding displacement field in the y-direction while

Figure 4-d shows the field of displacement in the y-direction obtained from FE simulation. To further analyse the behaviour of the crystal, Figure 5-a shows the displacement profile in the x-direction along the middle vertical grid of the plate, while Figure 5-b shows the displacement profile in the y-direction along the middle horizontal grid of the plate. Again, FE results are presented alongside the results from the proposed model in Figure 5-a and Figure 5-b, respectively. Comparison of these results reveals a good degree of agreement between the predictions obtained from the proposed NOSBPD model and the results of simulation from the FEM for the same problem. The correspondence of results between the two methods demonstrates the accuracy and reliability of the proposed model in capturing the behaviour of the ice crystal.

6.0 CONCLUSION

This paper presents a new approach to modelling single crystal S2 ice using the NOSBPD. The aim of this study was to develop a modelling framework that allows for a deeper understanding of the complex response of ice, considering nonlocal mechanisms like damage, size effects, and discontinuous behaviour such as fracture. These phenomena are difficult to capture using traditional continuum mechanics, necessitating the exploration of alternative approaches.

The results from simulation obtained from the proposed non-ordinary state-based peridynamic model show excellent agreement with those obtained from the well-established FE simulation. The displacement fields observed in the x and y directions exhibit consistent patterns and behaviours, closely matching the results from the FE method. This strong agreement between the two simulation approaches demonstrates the reliability and accuracy of the proposed model in capturing the response of ice.

By providing a reliable and efficient numerical framework with extended capabilities such as peridynamics offers, the proposed model opens new possibilities for studying the behaviour of ice crystals and analysing their complex response to external forces. This deeper understanding can lead to improved designs and more accurate predictions, ultimately enhancing the safety and reliability of structures and systems operating in icy conditions.

ACKNOWLEDGMENTS

The first author is supported by the government of the federal republic of Nigeria through the Petroleum Technology Development Fund (PTDF).

7.0 REFERENCES

Buryachenko, V. A. (2019). Computational homogenization in linear elasticity of peristatic periodic structure composites. *Mathematics and Mechanics of Solids*, *24*(8), 2497-2525. https://doi.org/10.1177/1081286518768039

Chen, X., & Gunzburger, M. (2011). Continuous and discontinuous finite element methods for a peridynamics model of mechanics. *Computer Methods in Applied Mechanics and*

Engineering, *200*(9), 1237-1250. https://doi.org/https://doi.org/10.1016/j.cma.2010.10.014

Elvin, A. A. (1996). Number of grains required to homogenize elastic properties of polycrystalline ice. *Mechanics of Materials*, *22*(1), 51-64. https://doi.org/https://doi.org/10.1016/0167-6636(95)00024-0

Evangelatos, G. I., & Spanos, P. D. (2011). A collocation approach for spatial discretization of stochastic peridynamic modeling of fracture. *6*(7-8), 1171-1195. https://doi.org/10.2140/jomms.2011.6.1171

Galadima, Y., Oterkus, E., & Oterkus, S. (2019). Two-dimensional implementation of the coarsening method for linear peridynamics. *AIMS Material Science*, *6*(2), 252-275. https://doi.org/http://dx.doi.org/10.3934/matersci.2019.2.252

Galadima, Y. K., Oterkus, E., & Oterkus, S. (2020a). Investigation of the effect of shape of inclusions on homogenized properties by using peridynamics. *Procedia Structural Integrity*, *28*, 1094-1105. https://doi.org/10.1016/j.prostr.2020.11.124

Galadima, Y. K., Oterkus, E., & Oterkus, S. (2020b). Model order reduction of linear peridynamic systems using static condensation. *Mathematics and Mechanics of Solids*, 1081286520937045.

Galadima, Y. K., Oterkus, E., & Oterkus, S. (2022). Static condensation of peridynamic heat conduction model. *Mathematics and Mechanics of Solids*, *0*(0), 10812865221081160. https://doi.org/10.1177/10812865221081160

Galadima, Y. K., Oterkus, S., Oterkus, E., Amin, I., El-Aassar, A.-H., & Shawky, H. (2023a). Modelling of viscoelastic materials using non-ordinary state-based peridynamics. *Engineering with Computers*. https://doi.org/10.1007/s00366-023-01808-9

Galadima, Y. K., Oterkus, S., Oterkus, E., Amin, I., El-Aassar, A.-H., & Shawky, H. (2023b). A Nonlocal Method to Compute Effective Properties of Viscoelastic Composite Materials Based on Peridynamic Computational Homogenization Theory. *Composite Structures*.

Galadima, Y. K., Xia, W., Oterkus, E., & Oterkus, S. (2021). Chapter 17 - Multiscale modeling with peridynamics. In E. Oterkus, S. Oterkus, & E. Madenci (Eds.), *Peridynamic Modeling, Numerical Techniques, and Applications* (pp. 371-386). Elsevier. https://doi.org/https://doi.org/10.1016/B978-0-12-820069-8.00018-4

Galadima, Y. K., Xia, W., Oterkus, E., & Oterkus, S. (2022). Peridynamic computational homogenization theory for materials with evolving microstructure and damage. *Engineering with Computers*. https://doi.org/10.1007/s00366-022-01696-5

Li, J., Wang, C., Wang, Q., Zhang, Y., Jing, C., & Han, D. (2023). Peridynamic modeling of polycrystalline S2 ice and its applications. *Engineering Fracture Mechanics*, *277*, 108941. https://doi.org/https://doi.org/10.1016/j.engfracmech.2022.108941

Liu, M., Wang, Q., & Lu, W. (2017). Peridynamic simulation of brittle-ice crushed by a vertical structure. *International Journal of Naval Architecture and Ocean Engineering*, *9*(2), 209-218. https://doi.org/https://doi.org/10.1016/j.ijnaoe.2016.10.003

Lu, W., Li, M., Vazic, B., Oterkus, S., Oterkus, E., & Wang, Q. (2020). Peridynamic Modelling of Fracture in Polycrystalline Ice. *Journal of Mechanics*, *36*(2), 223-234. https://doi.org/10.1017/jmech.2019.61

Nguyen, C. T., & Oterkus, S. (2020). Ordinary state-based peridynamic model for geometrically nonlinear analysis. *Engineering Fracture Mechanics*, *224*, 106750. https://doi.org/https://doi.org/10.1016/j.engfracmech.2019.106750

Oterkus, E., Guven, I., & Madenci, E. (2012). Impact damage assessment by using peridynamic theory. *Central European Journal of Engineering*, *2*(4), 523-531. https://doi.org/10.2478/s13531-012-0025-1

Oterkus, E., Madenci, E., Weckner, O., Silling, S., Bogert, P., & Tessler, A. (2012). Combined finite element and peridynamic analyses for predicting failure in a stiffened composite curved panel with a central slot. *Composite Structures*, *94*(3), 839-850. https://doi.org/https://doi.org/10.1016/j.compstruct.2011.07.019

Parks, M. L., Lehoucq, R. B., Plimpton, S. J., & Silling, S. A. (2008). Implementing peridynamics within a molecular dynamics code. *Computer Physics Communications*, *179*(11), 777-783. https://doi.org/https://doi.org/10.1016/j.cpc.2008.06.011

Silling, S. A. (2000). Reformulation of elasticity theory for discontinuities and long-range forces. *Journal of the Mechanics and Physics of Solids*, *48*(1), 175-209. https://doi.org/https://doi.org/10.1016/S0022-5096(99)00029-0

Silling, S. A. (2011). A Coarsening Method for Linear Peridynamics. *9*(6), 609-622. https://doi.org/10.1615/IntJMultCompEng.2011002674

Silling, S. A., & Askari, E. (2005). A meshfree method based on the peridynamic model of solid mechanics. *Computers & Structures*, *83*(17), 1526-1535. https://doi.org/https://doi.org/10.1016/j.compstruc.2004.11.026

Silling, S. A., Epton, M., Weckner, O., Xu, J., & Askari, E. (2007). Peridynamic States and Constitutive Modeling. *Journal of Elasticity*, *88*(2), 151-184. https://doi.org/10.1007/s10659-007-9125-1

Song, Y., Yan, J., Li, S., & Kang, Z. (2019). Peridynamic Modeling and Simulation of Ice Craters By Impact. *Computer Modeling in Engineering \& Sciences*, *121*(2), 465--492. http://www.techscience.com/CMES/v121n2/36312

Vazic, B., Oterkus, E., & Oterkus, S. (2020). In-Plane and Out-of Plane Failure of an Ice Sheet using Peridynamics. *Journal of Mechanics*, *36*(2), 265-271. https://doi.org/10.1017/jmech.2019.65

Wang, H., & Tian, H. (2012). A fast Galerkin method with efficient matrix assembly and storage for a peridynamic model. *Journal of Computational Physics*, *231*(23), 7730-7738. https://doi.org/https://doi.org/10.1016/j.jcp.2012.06.009

Wang, H., & Tian, H. (2014). A fast and faithful collocation method with efficient matrix assembly for a two-dimensional nonlocal diffusion model. *Computer Methods in Applied Mechanics and Engineering*, *273*, 19-36. https://doi.org/https://doi.org/10.1016/j.cma.2014.01.026

West, B., O'Connor, D., Parno, M., Krackow, M., & Polashenski, C. (2022). Bonded Discrete Element Simulations of Sea Ice With Non-Local Failure: Applications to Nares Strait. *Journal of Advances in Modeling Earth Systems*, *14*(6), e2021MS002614. https://doi.org/https://doi.org/10.1029/2021MS002614

Xia, W., Galadima, Y., Oterkus, E., & Oterkus, S. (2019). Representative volume element homogenization of a composite material by using bond-based peridynamics. *Journal of Composites and Biodegradable Polymers*.

Xia, W., Oterkus, E., & Oterkus, S. (2021). Ordinary state-based peridynamic homogenization of periodic micro-structured materials. *Theoretical and Applied Fracture Mechanics*, *113*, 102960. https://doi.org/https://doi.org/10.1016/j.tafmec.2021.102960

Xue, Y., Liu, R., Liu, Y., Zeng, L., & Han, D. (2019). Numerical Simulations of the Ice Load of a Ship Navigating in Level Ice Using Peridynamics. *Computer Modeling in Engineering \& Sciences*, *121*(2), 523--550. http://www.techscience.com/CMES/v121n2/36315